PNL-3137
UC-70

Numerical Modeling of Liquid Feeding in the Liquid-Fed Ceramic Melter

R. L. Hjelm
T. E. Donovan

October 1979

Prepared for the U.S. Department of Energy
under Contract EY-76-C-06-1830

Pacific Northwest Laboratory
Operated for the U.S. Department of Energy
by Battelle Memorial Institute

PNL-3137

NOTICE

PACIFIC NORTHWEST LABORATORY
operated by
BATTELLE
for the
UNITED STATES DEPARTMENT OF ENERGY
Under Contract EY-76-C-06-1830

Printed in the United States of America
Available from
National Technical Information Service
United States Department of Commerce
5285 Port Royal Road
Springfield, Virginia 22151

Price: Printed Copy $____*; Microfiche $3.00

*Pages	NTIS Selling Price
001-025	$4.00
026-050	$4.50
051-075	$5.25
076-100	$6.00
101-125	$6.50
126-150	$7.25
151-175	$8.00
176-200	$9.00
201-225	$9.25
226-250	$9.50
251-275	$10.75
276-300	$11.00

PNL-3137
UC-70

NUMERICAL MODELING OF LIQUID FEEDING IN THE LIQUID-FED CERAMIC MELTER

R. L. Hjelm
T. E. Donovan

October 1979

Prepared for the
U.S. Department of Energy
under Contract EY-76-C-06-1830

Pacific Northwest Laboratory
Richland, Washington 99352

SUMMARY

A modeling scheme developed by the Pacific Northwest Laboratory numerically simulates the behavior of the Liquid-Fed Ceramic Melter (LFCM) during liquid feeding. The computer code VECTRA (Vorticity Energy Code for TRansport Analysis) was used to simulate the LFCM in the idling and liquid feeding modes. Results for each simulation include molten glass temperature profiles and isotherm contour plots, stream function contour plots, heat generation rate contour plots, refractory isotherms, and heat balances.

The results indicated that the model showed no major deviations from real LFCM behavior and that high throughput should be attainable. They also indicated that reboil was a possibility as a steady liquid feeding state was approached, very steep temperature gradients exist in the Monofrax K-3, and that phase separation could occur in the bottom corners during liquid feeding and over the entire floor while idling.

CONTENTS

FIGURES

NUMERICAL MODELING OF LIQUID FEEDING OF THE LIQUID-FED CERAMIC MELTER

INTRODUCTION

This report describes a modeling scheme developed at the Pacific Northwest Laboratory (PNL) to numerically simulate the behavior of the Liquid-Fed Ceramic Melter (LFCM) while directly feeding simulated liquid high level wastes. The LFCM[1] is an integral part of the High Level Waste Immobilization Process currently under development at PNL for the U.S. Department of Energy (DOE).

The extreme environment in the melter substantially limits observation and direct measurement efforts to obtain information about the molten glass behavior. In addition, physical changes in the LFCM are costly, thus inhibiting direct experimentation with the actual melter. For these reasons, numerical modeling can be a valuable adjunct in documenting and explaining the physical processes of the molten glass. Further, it can provide operating and design information to support the melter development work.

The PNL-developed computer code VECTRA was used in this study to simulate the LFCM in two operating modes. VECTRA is a two-dimensional code that can solve the vorticity, stream function, energy, and electric field equations in a wide variety of geometries.[2] The code had been used previously to simulate molten glass flows.[3] Numerical results generated by the code have been compared with good agreement to measurements taken on the LFCM physical model.[4] For these reasons, VECTRA was used to simulate the LFCM in both the idling and liquid feed modes. The objective was to observe and understand the similarities and differences in LFCM behavior in both cases.

This report briefly summarizes how the LFCM operates, to provide the background necessary to the feeding and idling model descriptions. Results of the idling and feeding simulations are then documented. The final sections discuss the simulation results and conclusions.

FEEDING AND IDLING MODELS

As background, LFCM operation is briefly described first in this section. The models used to simulate the LFCM idling and liquid feeding modes are then presented.

LIQUID-FED CERAMIC MELTER OPERATION

In the High Level Waste Immobilization process, the waste is mixed with glass additives and melted to produce a stable glass product suitable for long-term storage in metal canisters. The LFCM heats the molten glass by passing an electric current through it. The current is supplied by electrodes placed on opposing melter walls. The LFCM has two independent sets of electrodes: a lower set along the melter floor and an upper set 4 in. above the lower set. Because the two electrode sets are independent, the ratio of the power input through the upper set to the power input through the lower set (power skew) can be varied. At the LFCM operating temperature, the glass has the properties of an electrically conductive fluid. The heat loss through the melter sides cools the glass adjacent to the walls, causing it to become denser and sink to the bottom. This sinking motion establishes a circulation pattern in the glass melter. Thus, the hydrodynamic behavior in the melter is coupled to its electric and thermodynamic characteristics.

The behavior of the LFCM is significantly different during liquid feeding than while idling (no feeding).[5,6] While idling, the glass melt is entirely molten, with the top of the glass transferring heat by radiation up across an air gap to the melter lid. While feeding, cold liquid is poured directly onto the hot glass melt. During a steady feeding state, a crust (cold cap) exists on top of the glass melt. Above this cold cap is a layer of liquid at the liquid boiling temperature ($\sim 150^{\circ}C$). Thus, heat transfer by radiation at the glass batch top is negligible during liquid feeding. In addition, because of throughput during feeding, the required power input is much larger than that required to maintain the glass at operating temperature ($1200^{\circ}C$) during idling.

FEEDING AND IDLING MODELS

Because the top of the glass melt changes with operating mode, different models are required to simulate the LFCM during idling and during liquid feeding. A schematic of the system simulated by VECTRA for the liquid feeding case is shown in Figure 1a; that for the idling case is shown in Figure 1b. Only half of each cross section is shown, because the LFCM is symmetric in that plane. However, the entire cross section was simulated by VECTRA.

The refractory walls surrounding the glass melt, as well as the electrodes and the boundary conditions, are the same in both the idling and liquid feeding models. Differences exist at the top of the glass melt. For the idling case, a radiation boundary at the top of the glass melt transfers heat by radiation from the molten glass, across the vapor gap, to the Kaowool insulation lid. The Kaowool insulation lid in turn transfers heat by radiation and conduction to the ambient atmosphere above it.

For the liquid feeding case, a uniform batch crust 2 in. thick is established at the top of the glass melt. The thermal conductivity of this crust is assumed to be 0.5 Btu/hr-ft-^{o}F, based on the measured value for glass at 700^{o}C. The bottom of this crust acts as a no-slip boundary for the molten glass below. There is little data available on the actual structure or properties of the batch crust in the LFCM. The above assumptions are made based on the available information, but it is nearly impossible to validate these idealizations required to perform the analysis. The feed into the glass melt is assumed to occur at the bottom of the batch crust. The outflow is assumed to occur at the center of the melter floor. In the actual LFCM, the outflow takes place on a wall outside the plane simulated by VECTRA. To conserve mass in the simulation, it is necessary to place the outflow along the melter floor. Above the batch crust is a 0.5-in. thick liquid layer held at a constant, uniform temperature of 150^{o}C. This temperature is assumed to be the boiling temperature of the liquid feed. To account for endothermic reactions that take place in the batch crust, a heat sink totalling -2 kW is applied to the crust.

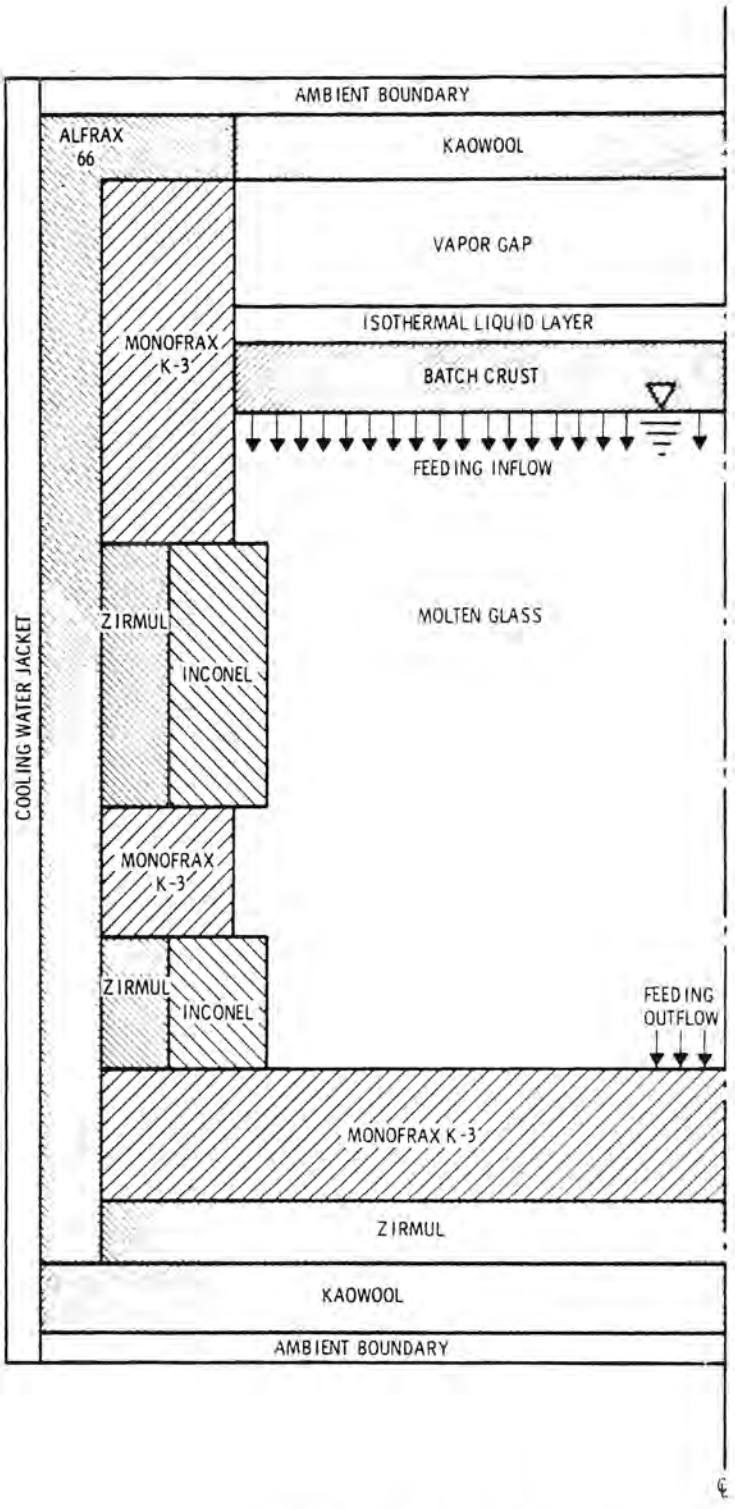

a. Liquid Feeding Mode

FIGURE 1. Schematic of Model Used to Simulate LFCM

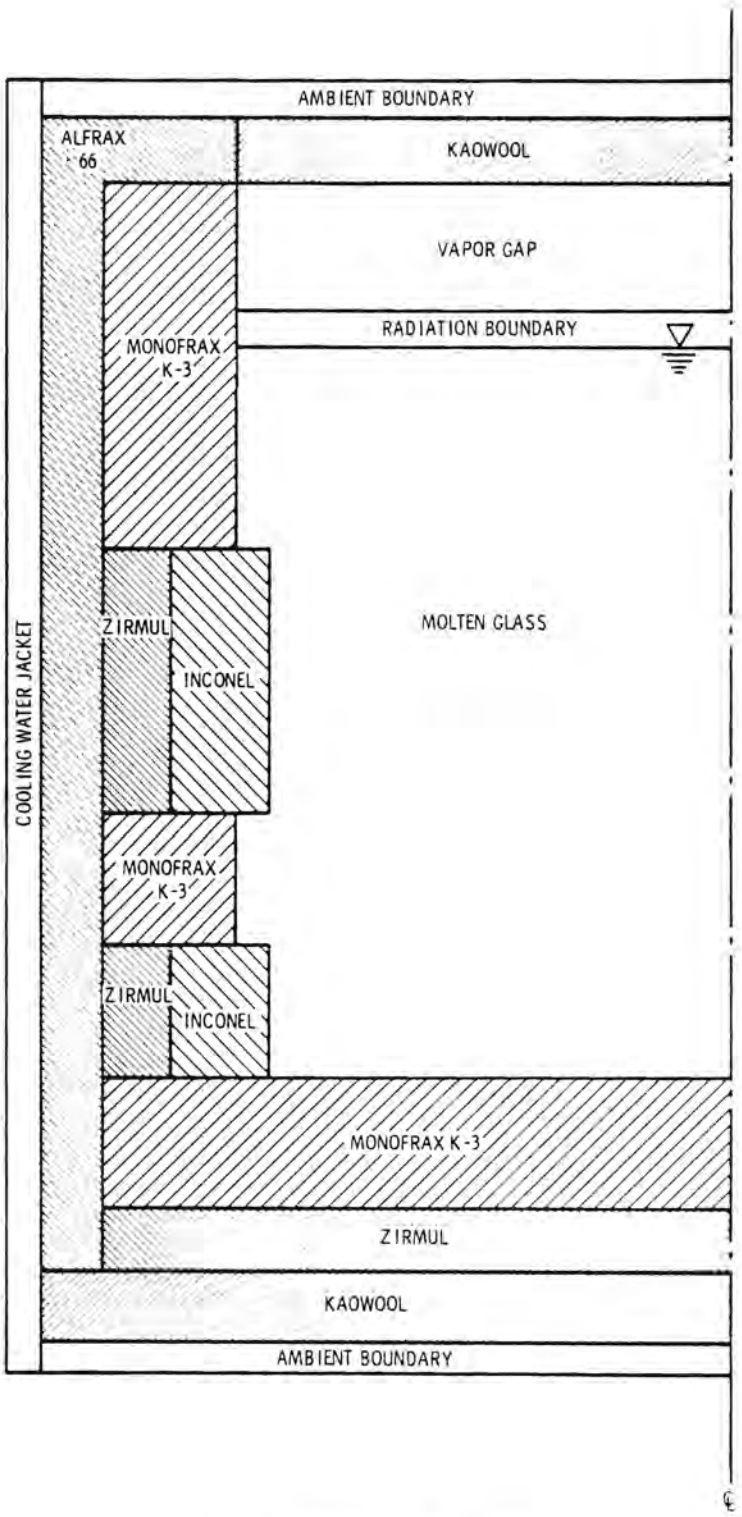

b. Idling Mode

FIGURE 1. (contd)

RESULTS

The idling and liquid feeding simulations were executed by VECTRA until a steady energy state was reached, i.e., until the heat transfer out of the system equaled the power input. (As described in Reference 3, the flow field never achieves a steady state.) The controlling parameter for each case was the electrode temperature. An electrode temperature of 1050°C was the goal because this is the temperature control point in actual operation. For idling, the result was 1049°C; for liquid feeding, the electrode temperature was 1062°C. The boundary temperatures for both cases were an ambient temperature of 27°C and a cooling jacket temperature of 38°C.

POWER REQUIREMENTS

The idling simulation of the LFCM required 9.5 kW/ft, or 27 kW total, to maintain the electrode temperature at 1050°C. Because of throughput and the isothermal boundary that accounts for heat of vaporization at the cold cap, the liquid feeding case required much more power to maintain an electrode temperature of 1050°C--29 kW/ft, or 82 kW overall. This latter value compares very well to the actual prototype power requirements of 90 kW for a similar feed rate. The power required for idling, 27 kW, is significantly less than that required in the actual LFCM. Two reasons for this difference are possible. First, the model assumes that there is no heat transfer in the direction perpendicular to the plane modeled. This is a poor but necessary assumption in two-dimensional modeling. Second, there is less insulation on the lid of the actual LFCM than was used in the model. Thus, the simulation assumed a better insulated melter than the actual LFCM. Both cases were run with 75% of the power input through the upper electrodes.

TEMPERATURES IN THE MELTING CAVITY

Figure 2 illustrates the temperature profile of the central portion of the melter from the floor up to the Kaowool lid. In the liquid feeding case (Figure 2a), the molten glass temperature is fairly uniform from the floor up

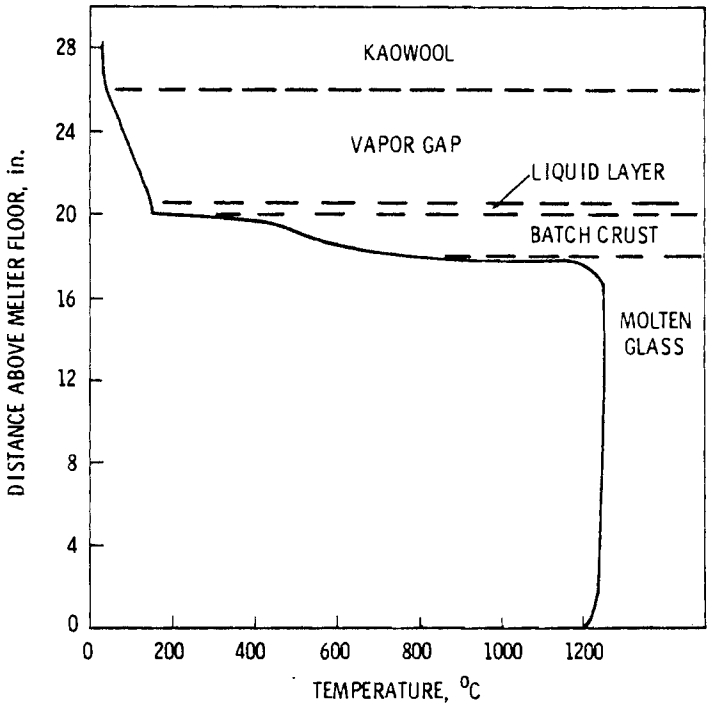

a. Liquid Feeding Mode

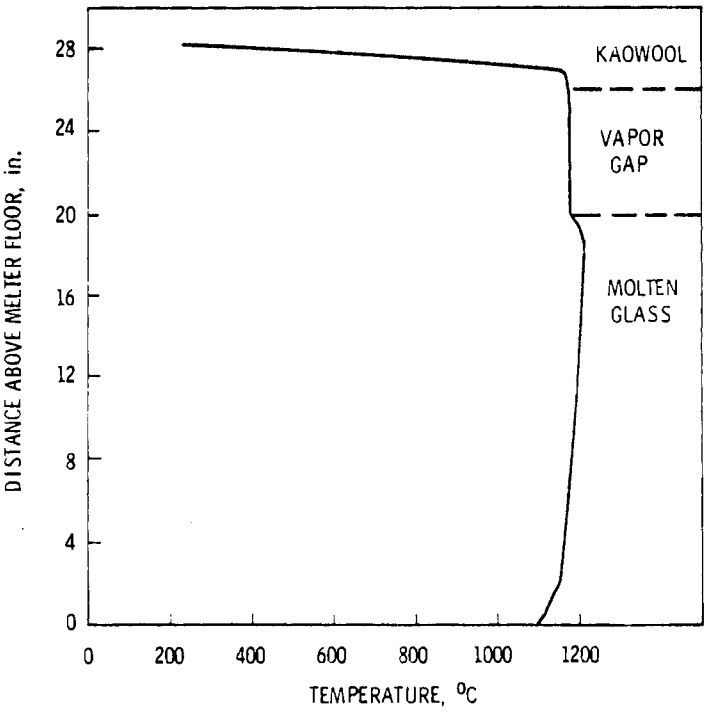

b. Idling Mode

FIGURE 2. Liquid-Fed Ceramic Melter Central Portion Temperature Profiles

to near the crust, where there is a very steep temperature gradient between the bulk glass and the crust. The interface temperature is computed to be 760°C, which is very close to the actual temperature at which glass begins to melt. This implies that the assumptions used to model the top of the molten glass during feeding work fairly well. The temperature continues to drop in the batch crust until the 150°C liquid layer is reached. Above the liquid layer the temperatures decline gradually to the ambient temperature.

The temperature profile while idling (Figure 2b) is significantly different from the liquid feeding case. The floor temperature is lower and a larger temperature gradient is present in the bottom part of the melter while idling. The fluid temperature is generally lower than while feeding. While idling, there is no crust above the glass melt, so the temperature peaks 18 in. above the floor and then cools slightly at the top of the melt. This surface then transfers heat by radiation to the lid. Notice that there is almost no temperature drop across the vapor gap. The temperature change between ambient and the glass melt top occurs almost entirely in the Kaowool lid insulation.

Figure 3 illustrates isotherms in the molten glass for the idling and feeding cases. Figure 3a, the feeding case, shows that the glass temperature is very uniform except in the bottom corners, where there are definite cold spots. The temperature drop from the floor center to the corners is about 80°C. In the idling case shown in Figure 3b, the isotherms illustrate a temperature gradient from the top of the melt to the bottom, but indicate that the glass temperature is nearly uniform along a traverse between electrodes. Thus, in the idling case, the entire floor is colder, instead of just the corners as in the feeding case.

FLOW FIELDS

Figure 4 presents stream function contour plots for the feeding and idling cases. The same values of the stream function are plotted for each case. The differences between Figure 4a and 4b indicate that the glass velocities in the feeding case are two to three times higher than in the idling

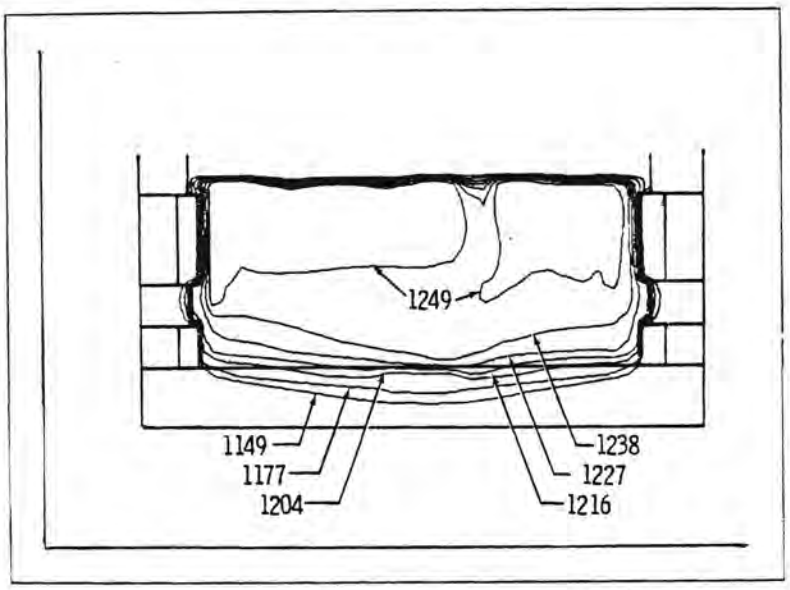

a. During Liquid Feeding

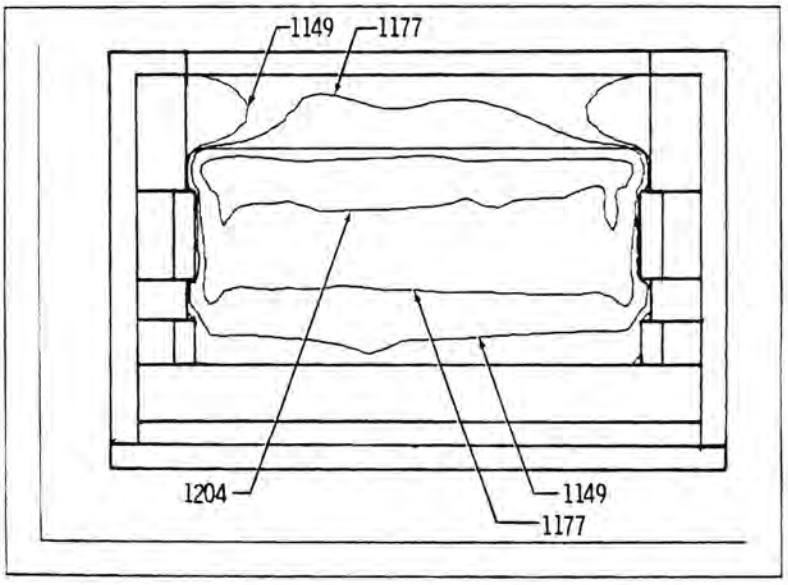

b. While Idling

FIGURE 3. Isotherms in Molten Glass (Contour Values in ^{o}C)

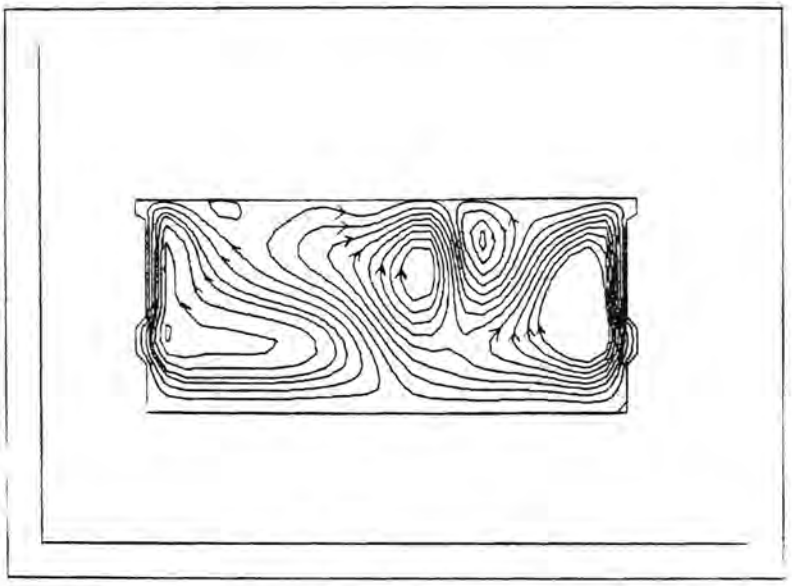

a. During Liquid Feeding

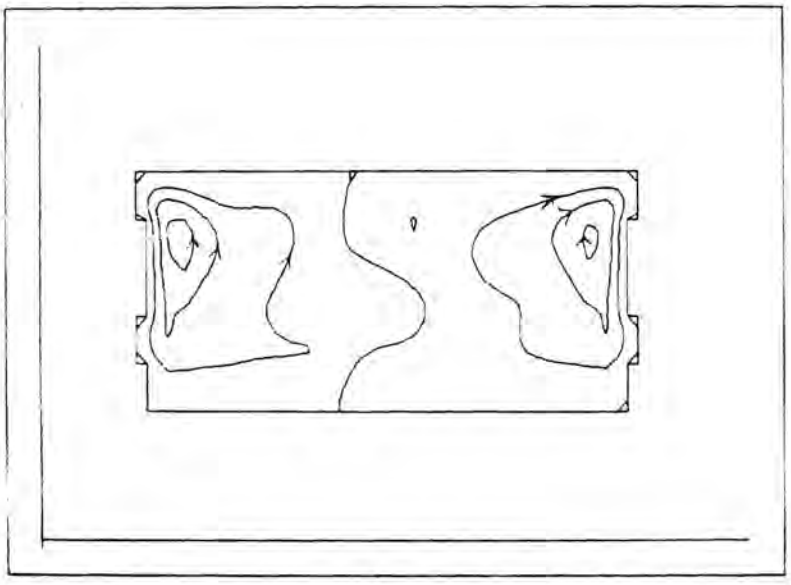

b. While Idling

FIGURE 4. Stream Function Contours

case. The steep temperature gradient at the glass melt top in the feeding case cools the glass there more, thus causing it to fall into the warmer glass below with greater velocity. Higher velocities for the feeding case lead to a better-mixed, more uniform temperature fluid. This helps explain why the glass is warmer in the bottom half of the melter during feeding.

HEAT GENERATION RATES

Because the power skew is the same for both idling and feeding cases, differences in only the temperature field will lead to differences in the heat generation field. Figure 5 illustrates the heat generation fields for liquid feeding and idling cases. The contours plotted are the local value of heat generation rate divided by the average heat generation rate. A comparison shows that heat is generated more uniformly in the feeding case because of more uniform glass temperatures. This is especially noticeable in the bottom center region of the melter. At the melter top, the feeding case heat generation rate drops, due to the steep temperature gradient there.

HEAT BALANCE

A heat balance performed for each case yielded the following results: for the idling case, 21.6 kW exit through the electrodes and bottom, with 2.3 kW through the bottom. For the feeding case, 21.8 kW exit through the electrodes and bottom, with 2.5 kW through the bottom. In the prototype LFCM, it is estimated that 20 kW are lost through the cooling jackets. The simulation results are in good agreement.

TEMPERATURES IN THE REFRACTORY

Figure 6 shows how the temperatures vary in the refractory surrounding the molten glass for the feeding and idling cases. In both cases, most of the temperature drop in the side walls occurs in the Monofrax K-3. The cooling jackets on the sides enhance cooling there. In the bottom refractory, there is a noticeable difference in the isotherms between the two cases--the bottom

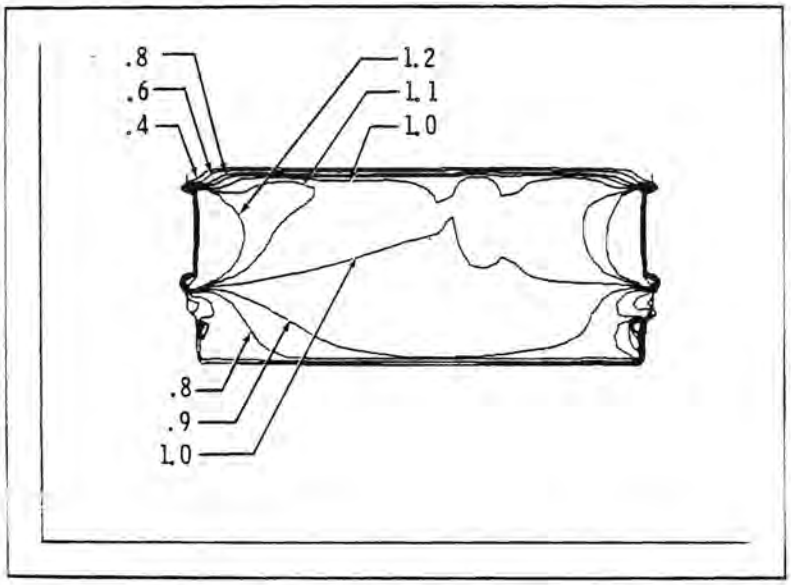

a. During Liquid Feeding

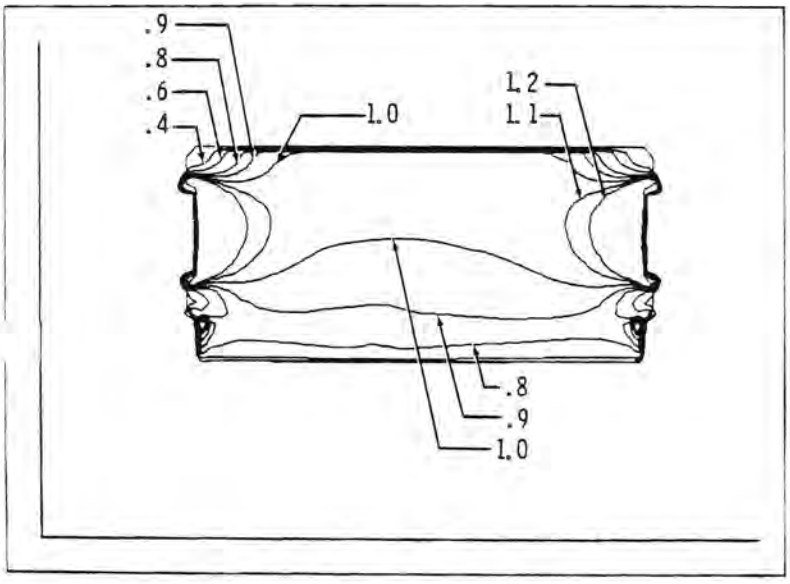

b. While Idling

FIGURE 5. Normalized Heat Generation Rate Contours

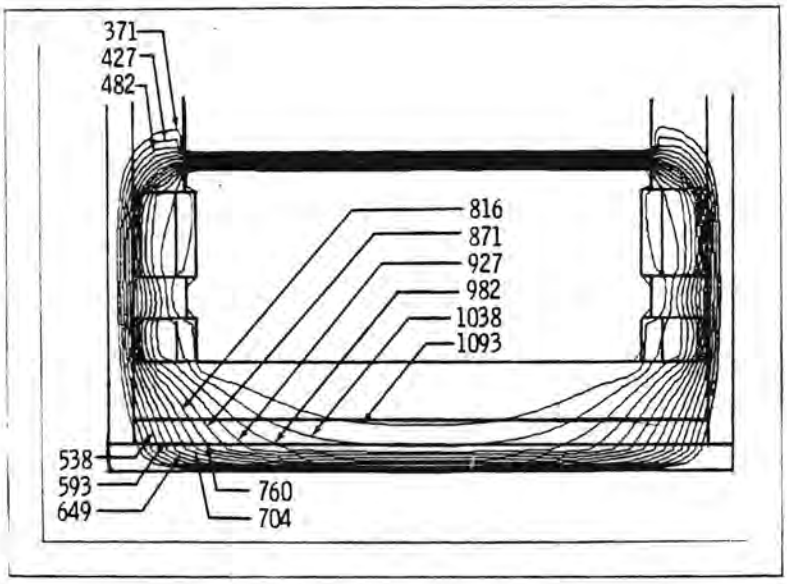

a. During Liquid Feeding

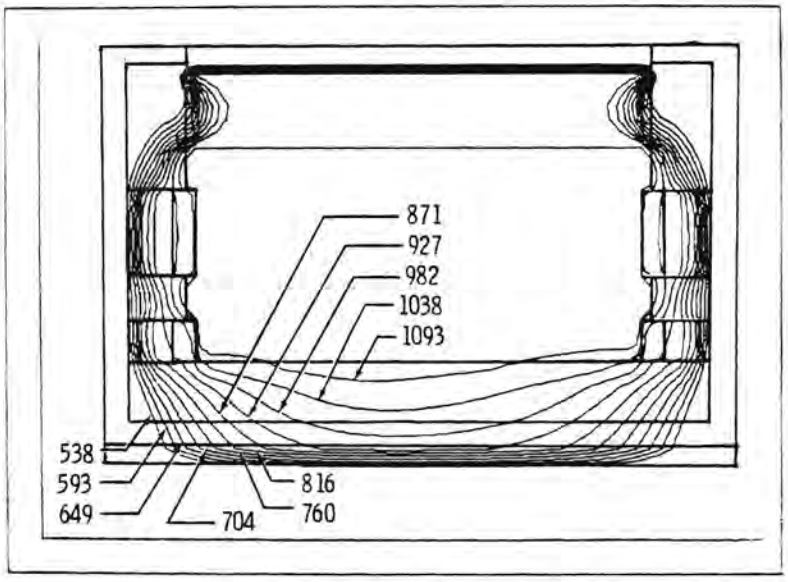

b. While Idling

FIGURE 6. Refractory Isotherms (Contour Values in ^{o}C)

refractory while feeding is warmer. This is a direct result of the warmer glass temperatures along the central floor region during feeding. Near the batch crust, there is a large temperature gradient in the Monofrax K-3. The peak value of the temperature gradient in the Monofrax K-3 is 573^{o}C/in. It occurs immediately below the batch crust, where the glass temperature gradient is steepest. In the idling case, there are no steep vertical temperature gradients, because there is no cold cap above the molten glass.

The temperatures computed in the floor refractory are much warmer than those measured in the actual LFCM. One reason for this result is that the model neglects heat transfer in the direction perpendicular to the plane modeled, i.e., the two-dimensional assumption. Another reason is that the model neglected the freeze valve[1] in the floor, which acts as a heat sink.

DISCUSSION

The results generated by the numerical simulation of the LFCM in the idling and feeding modes aid in understanding the physical processes of the molten glass. The findings also point out some potential problem areas in LFCM operation.

When switching from idling to feeding modes in the LFCM, the results indicate that the overall glass temperature will increase. This is a good indication that high throughputs are attainable. Another indication of high throughput possibilities is the high glass velocities observed during liquid feeding. High velocities decrease the time required for good mixing, which allows the feed rate to be increased. However, the temperature increase occuring in the feeding mode can result in reboil,[5,6] a sudden release of dissolved gases in the glass, which can turn it into a foam. Reboil can cause complete disruption of the cold cap, thus, precautions must be taken to avoid reboil.

The temperature contours in the refractory during liquid feeding indicate another potential problem area. Near the cold cap, the glass experiences extreme temperature changes in very short distances; large temperature gradients in the adjacent Monofrax K-3 result. The peak gradient, 573^{o}C/in., could lead to cracking in the refractory during steady-state, fully flooded operation. Temperature measurements should be taken in the prototype LFCM refractory to verify this result and determine whether or not corrective action is required.

During liquid feeding, the glass temperatures were fairly uniform, with potential cold spots in the bottom corners. With uniform temperatures, there is less chance of phase separation in the glass, i.e., crystals forming and building up along the floor. During idling, the entire LFCM floor area was cold relative to the bulk temperature, indicating a potential phase separation problem. The floor area would be warmer if a larger proportion of the total power were input through the lower electrodes. Skewing the heat generation toward the melter floor increases floor temperature and glass velocities along the floor.[3] Both consequences are desirable.

The validity of the results rests on the validity of the two major idealizations made in the analysis: 1) that the system is two-dimensional, and 2) that the cold cap can be simplified as was done here. There are obvious shortcomings to neglecting three-dimensional effects. Neglecting heat transfer in one direction results in less power required than in the prototype LFCM to maintain the same temperature. Neglecting wall effects on the fluid flow results in a flow field different from the real LFCM. In simulating the cold cap, the primary goal was to model the heat transfer properly by simplifying a very complex system with several assumptions. The numerical results do not exhibit any major deviations from the prototype LFCM behavior.

CONCLUSIONS

The modeling scheme developed to simulate the LFCM during liquid feeding has produced results that showed no major deviations from LFCM behavior. The results indicated positive operating conditions and pointed out some required precautionary measures. Higher fluid velocities and more uniform temperatures occur during liquid feeding, increasing homogeneity and capacity and reducing the possibility of phase separation. However, when switching to the liquid feeding mode from the idling state, glass temperatures will increase and can result in reboil. The results also indicate a high temperature gradient in the Monofrax K-3. A laboratory test should be performed to verify this result. Finally, inputting a larger percentage of power through the lower electrodes will raise temperatures along the floor during idling and help eliminate the possibility of phase separation.

It is concluded that the numerical model can predict trends in the LFCM. Thus, comparisons between the LFCM idling and liquid feeding modes performed in this study are reasonable.

REFERENCES

1. J. L. Buelt and C. C. Chapman, Liquid Fed Ceramic Melter: A General Description Report. PNL-2735, Pacific Northwest Laboratory, Richland, WA 99352, October 1978.

2. D. S. Trent, A Numerical Model for Two-Dimensional Hydrodynamics and Energy Transport. BNWL-1803, Pacific Northwest Laboratory, Richland, WA 99352, June 1973.

3. R. L. Hjelm and T. E. Donovan, "A Numerical Investigation of Electric Field Effects on Unsteady Buoyant Molten Glass Flows," ASME Publication 79-HT-98, American Society of Mechanical Engineers, New York, NY 10017, August 1979.

4. M. S. Quigley and D. K. Kreid, Physical Modeling of Joule Heated Ceramic Glass Melters for High Level Waste Immobilization. PNL-2809, Pacific Northwest Laboratory, Richland, WA 99352, March 1979.

5. J. L. Buelt, C. C. Chapman, S. M. Barnes, and R. D. Dierks, "A Review of Continuous Ceramic-Lined Melters and Associated Experience at PNL." PNL-SA-7590, Presented at the International Symposium on Ceramics in Nuclear Waste Management, sponsored by the Nuclear Division of the American Ceramic Society and the U.S. Department of Energy, Cincinnati, Ohio, April 30-May 3, 1979.

6. J. L. Buelt and C. C. Chapman, "Slurry Feeding of Nuclear Waste to an Electric Glass Melter," PNL-SA-7571, Presented at the 50th Annual American Nuclear Society Meeting, Atlanta, Georgia, June 5, 1979.

DISTRIBUTION

No. of Copies

UNITED STATES

A. A. Churm
DOE Chicago Patent Group
9800 South Cass Ave.
Argonne, IL 60439

R. E. Cunningham
Deputy Director for Fuels and Materials
Nuclear Regulatory Commission
Silver Springs, MD 20910

T. C. Chee
DOE Office of Nuclear Waste Management
Washington, DC 20545

C. R. Cooley
DOE Office of Nuclear Waste Management
Washington, DC 20545

Sheldon Meyers
DOE Office of Nuclear Waste Management
Washington, DC 20545

R. G. Romatowski
DOE Office of Nuclear Waste Management
Washington, DC 20545

C. A. Heath
DOE Office of Nuclear Waste Management
Washington, DC 20545

G. Oertel
DOE Office of Nuclear Waste Management
Washington, DC 20545

No. of Copies

A. F. Perge
DOE Office of Nuclear Waste Management
Washington, DC 20545

R. D. Walton
DOE Office of Nuclear Waste Management
Washington, DC 20545

J. Neff, Program Manager
Department of Energy
Columbus Program Office
505 King Avenue
Columbus, OH 43201

John Van Cleve
DOE Oak Ridge Operations Office
P.O. Box X
Oak Ridge, TN 37830

E. S. Goldberg
DOE Savannah River Operations Office
P.O. Box A
Aiken, SC 29801

27 DOE Technical Information Center

J. R. Berreth
Allied Chemical Corporation
550 2nd Street
Idaho Falls, ID 83401

Allied Chemical Corporation
(File Copy)
550 2nd Street
Idaho Falls, ID 83401

No. of
Copies

A. Williams
Allied-General Nuclear Service
P.O. Box 847
Barnwell, SC 29812

J. L. Jardine
Argonne National Laboratory
9700 South Cass Avenue
Argonne, IL 60439

M. M. Steindler/L. E. Trevorrow
Argonne National Laboratory
9700 South Cass Avenue
Argonne, IL 60439

Wayne Carbiener
Battelle Memorial Institute
505 King Ave.
Columbus, OH 43201

J. Kircher
Office of Nuclear Waste Isolation
Battelle Memorial Institute
505 King Ave.
Columbus, OH 43201

B. Rawls
Office of Nuclear Waste Isolation
Battelle Memorial Institute
505 King Ave.
Columbus, OH 43201

Brookhaven National Laboratory
Reference Section
Information Division
Upton, NY 11973

J. L. Crandall
E. I. duPont DeNemours and Company
Savannah River Laboratory
Aiken, SC 29801

H. L. Hull
E. I. duPont DeNemours and Company
Savannah River Laboratory
Aiken, SC 29801

No. of
Copies

R. G. Garvin
E. I. duPont DeNemours and Company
Savannah River Laboratory
Aiken, SC 29801

D. L. McIntosh
E. I. duPont DeNemours and Company
Savannah River Laboratory
Aiken, SC 29801

J. A. Kelley
E. I. duPont DeNemours and Company
Savannah River Laboratory
Aiken, SC 29801

M. D. Boersma
E. I. duPont DeNemours and Company
Savannah River Laboratory
Aiken, SC 29801

S. Mirshak
E. I. duPont DeNemours and Company
Savannah River Laboratory
Aiken, SC 29801

A. S. Jennings
E. I. duPont DeNemours and Company
Savannah River Laboratory
Aiken, SC 29801

H. Henning
Electric Power Research Institute
3412 Hillview Avenue
P.O. Box 10412
Palo Alto, CA 94301

Environmental Protection Agency
Technology Assessment Division
(AW-559)
Office of Radiation Programs
Washington, DC 20460

R. G. Barnes
General Electric Company
175 Curtner Avenue (M/C 858)
San Jose, CA 95125

No. of Copies

Los Alamos Scientific Laboratory (DOE)
P.O. Box 1663
Los Alamos, NM 87544

J. P. Duckworth
Plant Manager
Nuclear Fuel Services, Inc.
P.O. Box 124
West Valley, NY 14171

J. G. Cline, General Manager
NYS Energy Research and Development Authority
230 Park Avenue, Rm 2425
New York, NY 10017

Oak Ridge National Laboratory (DOE)
Central Research Library
Document Reference Section
P.O. Box X
Oak Ridge, TN 37830

E. H. Kobisk
Solid State Division
Oak Ridge National Laboratory
Oak Ridge, TN 37830

R. Roy
Pennsylvania Stata University
Materials Research Laboratory
University Park, PA 16802

W. Weart
Sandia Laboratories
Albuquerque, NM 87107

J. O. Blomeke
Union Carbide Corporation (ORNL)
Chemical Technology Division
P. O. Box Y
Oak Ridge, TN 37830

R. E. Blanco
Union Carbide Corporation (ORNL)
Chemical Technology Division
P. O. Box Y
Oak Ridge, TN 37830

No. of Copies

D. E. Ferguson
Union Carbide Corporation (ORNL)
Chemical Technology Division
P. O. Box Y
Oak Ridge, TN 37830

H. W. Godbee
Union Carbide Corporation (ORNL)
Chemical Technology Division
P. O. Box Y
Oak Ridge, TN 37830

FOREIGN

2 International Atomic Energy Agency
Kartner Ring 11
P.O. Box 590
A-1011, Vienna, AUSTRIA

B. Morris
Atomic Energy Research Establishment,
Harwell, Didcot,
Berks, ENGLAND

D. W. Clelland
United Kingdom Atomic Energy Authority
Risley, ENGLAND

E. R. Merz
Institut fur Chemische Technologie
Kernforschungsanloge Julich GmbH
D517 Julich
Postfach 365
Federal Republic
WEST GERMANY

R. Bonniaud
Center de Marcoule
B.P. 170
30200 Baguols-sur-Ceze
FRANCE

No. of
Copies

C. Sombret
Centre de Marcoule
B.P. 170
30200 Baguols-sur-Ceze
FRANCE

F. Laude
Centre de Marcoule
B.P. 170
30200 Baguols-sur-Ceze
FRANCE

H. Krause
Kernforschungszentrum Karlsruhe
GmbH (KfK)
Postfach 3640
D7500 Karlsruhe
WEST GERMANY

S. Tashiro
Japan Atomic Energy Research
Institute
Environmental Safety Research
Laboratory
1-1-13, Shibashi
Minatopku, Tokyo
JAPAN

ONSITE

3 DOE Richland Operations Office

P. A. Craig
H. E. Ransom
M. J. Zamorski

5 Rockwell Hanford Operations

L. Brown
M. J. Kupfer
G. Reep
D. D. Wodrich
File Copy

Exxon Nuclear Company

S. J. Beard

No. of
Copies

Westinghouse Hanford Company

A. G. Blasewitz

66 Pacific Northwest Laboratory

S. M. Barnes
W. J. Bjorklund
H. T. Blair
W. F. Bonner
R. A. Brouns
J. L. Buelt
L. A. Chick
A. J. Currie
T. E. Donovan (10)
R. D. Dierks
M. S. Hanson
R. L. Hjelm (10)
L. K. Holton
J. H. Jarrett
D. E. Knowlton
D. K. Kreid
W. L. Kuhn
D. E. Larson
S. A. McCullough
J. L. McElroy (3)
G. B. Mellinger
J. E. Mendel
F. A. Miller
R. E. Nightingale
D. E. Olesen
K. H. Oma
C. R. Palmer
A. M. Platt
D. L. Prezbindowski (2)
M. S. Quigley
W. A. Ross
J. M. Rusin
D. H. Siemens
S. C. Slate
A. M. Sutey
C. L. Timmerman
R. T. Treat
D. S. Trent
Technical Information (5)
Publishing Coordination KE(2)